Matter in the Local Universe

L. da Costa
European Southern Observatory, Karl-Schwarzschild Strasse 2, D-85748, Garching bei München, Germany

Abstract. In this contribution we review the large body of work carried out over the past two decades to probe the dark matter in the local universe using redshift survey and peculiar velocity data. While redshift surveys have evolved rapidly over the years, gathering suitable peculiar velocity data and understanding the short-comings of different analyses have proven to be a difficult task. These difficulties have led to conflicting results which have casted some doubts on the usefulness of cosmic flows to constrain cosmological models. Recently, however, a consistent picture seems to be finally emerging with various methods of analyses applied to different data sets yielding concordant results. These favor a low-density universe, with constraints which are in good agreement with those obtained from LSS, high-redshift supernovae and CMB studies.

1 Introduction

LSS studies of the nearby universe are arguably ideal to address the question posed by the title of this conference. Indeed, if all the mass in the universe were locked into galaxies, complete redshift surveys of galaxies would provide the data required to fully characterize the matter distribution. However, we have learned that the luminous matter associated to galaxies represents a small fraction of the mass density of the universe, and that galaxies may be biased relative to the underlying distribution of matter. Still, if structures grow as a result of gravity alone, observation of the peculiar velocity of galaxies provides the means to probe the distribution of the total matter. In the standard picture for the formation of cosmic structures via gravitational instability the peculiar velocity of a galaxy is generated by fluctuations in the mass distribution. For galaxies outside virialized systems, linear perturbation theory predicts

$$\mathbf{v}(\mathbf{r}) \approx \frac{\Omega^{0.6} H_o}{4\pi} \int d^3r' \delta_m \frac{(\mathbf{r}' - \mathbf{r})}{|\mathbf{r}' - \mathbf{r}|^3} \, . \tag{1}$$

This can also be expressed in the following differential form

$$\nabla \cdot \mathbf{v} = -\Omega^{0.6} \delta_m, \tag{2}$$

where Ω is the mass density parameter, H_o is the Hubble constant and δ_m is the mass density fluctuation field. If galaxies are fair tracers of the underlying mass distribution and galaxy biasing is linear then $\delta_g = b\delta_m$, where δ_g is the galaxy density contrast and b is the bias parameter for a given population of mass tracers. The above equations show that by mapping the peculiar velocity field one can determine the distribution of mass and measure the parameter $\beta = \Omega^{0.6}/b$ by comparing the reconstructed density field with that observed for galaxies or by comparing the measured velocity field with the predicted gravity field generated by fluctuations of the galaxy density field.

These simple ideas have been the underlying motivation for the major wide-angle redshift surveys of optical and infrared galaxies and the Tully-Fisher (TF) and $D_n - \sigma$ redshift-distance surveys conducted over the past two decades. In this contribution we review all of these efforts, giving special emphasis to the results obtained from recently completed redshift-distance surveys. In section 2, we briefly mention the redshift surveys that have contributed to our understanding of the local galaxy distribution and those which have played a major role in the analysis of peculiar velocity data. In Section 3, we review the redshift-distance surveys and the peculiar velocity catalogs that have been used to map the peculiar velocity field in the nearby universe. In section 4, the most recent surveys are used to reconstruct the velocity and density fields and to measure β. These results are also compared with those obtained in earlier works. Finally, in Section 5 we briefly summarize the current status of the field.

2 Galaxy Distribution

Over the past two decades the number of redshift surveys and redshift data has greatly increased and a complete review is beyond the scope of the present contribution and can be found elsewhere [42][13]. Here we point out two classes of surveys that have had a strong bearing on some of the issues discussed here. The first class consists of wide-angle, dense sampling surveys such as the CfA2 [20] and SSRS2 [10] which revealed for the first time the full complexity of the galaxy distribution. The discovery of extended, coherent wall-like structures and of large regions devoid of luminous matter with scales comparable to the survey depth represented a serious challenge to the prevailing theories of structure formation and evolution. Furthermore, these surveys probed relatively large volumes which allowed for reasonable estimates of the power-spectrum of the galaxy density fluctuations to be made for the first time [32][33][11]. Even though unable to reach very large scales, when COBE normalized, comparison with N-body simulations demonstrated that the results were consistent with a low-Ω cosmological model and an unbiased galaxy distribution. The PS was well described by a shape parameter $\Gamma = 0.2$, consistent with other determinations [34]. Attempts were also made to study the small-scale velocity field by analyzing the redshift-space distortions. However, the small number of independent structures within the sampled volume made the results extremely sensitive to shot-noise [29].

These early surveys were followed by the considerably deeper LCRS [39] which demonstrated unambiguously that the largest scales of inhomogeneities had finally been reached. Quantitative analyses of the LCRS, by and large confirmed earlier statistical results, albeit with considerably smaller errors. More recently, the first results of the 2dFGRS project have become available. The survey consists of over 100,000 galaxies to a depth comparable to the LCRS, allowing for precise measurements of redshift-space distortions and large-scale power spectrum. Analysis of the redshift distortions caused by large-scale infall velocities yields a value of $\beta_o = 0.43$ [35], where β_o refers to optical galaxies. Assuming a relative bias $b_o/b_I \sim 1.3$ between optical and *IRAS* galaxies this implies $\beta_I \sim 0.56$. The derived galaxy power-spectrum [36] was found to be well-represented by a shape parameter $\Gamma = 0.2$, in good agreement with previous determinations. These results provide important constraints on the mass power-spectrum which can later be compared with those obtained using cosmic flows to test for consistency.

The second class of redshift surveys worth mentioning in the present context is that involving galaxy samples extracted from the *IRAS* survey such as the 1.9 Jy[41], the 1.2 Jy[18] and the *PSCz* [38] redshift surveys. While sparsely sampling the galaxy distribution, these surveys provide a sky coverage unmatched by optical surveys. This all-sky coverage allows a more reliable determination of the gravity field induced by fluctuations of the galaxy density field which can be compared to the measured peculiar velocity field to estimate the parameter β.

From the above discussion, it is clear that by themselves redshift surveys are more useful for studying the properties of galaxies than as cosmological probes. However, combining them with redshift independent distances to map out the peculiar velocity field of galaxies and to predict the peculiar velocity field from galaxy density fluctuations provide powerful tools to probe the nature of the matter distribution and its relation with the galaxy distribution.

3 Mapping the Peculiar Velocity Field

The radial component of the peculiar velocity is given by

$$U = cz - d$$

where d is an estimate of the galaxy distance derived from a secondary distance indicator. Most of the available samples rely on the TF and Fundamental Plane relations for spirals and early-type galaxies, respectively, with typical errors in distance of $\sim 20\%$. However, samples based on distance indicators with significant smaller errors, such as those based on surface brightness fluctuations and nearby Type Ia supernovae, are slowly growing and have already been successfully used to measure β[44][37].

In contrast to the rapid growth of samples with complete redshift information, redshift-distance samples have been difficult to gather. There are various practical reasons for that. First, to ensure the uniformity of the data and of the sky coverage requires coordinated observations in both hemispheres. Second, TF distances require the measurement of the rotational velocity of the galaxy either from

Table 1: **Summary of Redshift-Distance Surveys**

Survey	N_{obj}	Type	Coverage
Aaronson *et al.*	300	spirals	all-sky
Tonry & Davis	300	early	north
7 Samurai	400	early	all-sky
Willick	320	spirals	Perseus-Pisces
Courteau *et al.*	380	Sb-Sc	north
Mathewson *et al.*	2000+	spirals	south
SFI	1300	Sbc-Sc	all-sky
ENEAR	1600	early	all-sky
Shellflow	300	Sb-Sc	all-sky

the HI line width, which can only be efficiently measured in the northern hemisphere, or from measurements of optical rotation curves, a challenging observation. Third, for early-type galaxies, high signal-to-noise spectra are required for accurate measurements of the velocity dispersion. Finally, both distance indicators require high-quality photometric data. Table 1 summarizes the redshift-distance surveys conducted to date. The table includes only wide-angle redshift-distance surveys and the number of objects is just indicative of the sample size. Not included are the various surveys conducted to measure distances and peculiar velocities of clusters of galaxies which have been used to constrain the amplitude of the bulk flow on very large scales.

Early studies [43][1] focused on the properties of the flow field near Virgo. However, it was soon realized that the assumption of a spherical infall was too restrictive and that Virgo alone could not explain the motion of the Local Group relative to the CMB. A major contribution to the field was the work of the 7 Samurai[26], the first to probe well beyond the local supercluster, albeit sparsely. Analyses of this sample led to startling results such as the measurement of a large amplitude bulk flow, and the discovery of the Great Attractor, a large mass concentration associated with the Hydra-Centaurus complex. Among the main conclusions of this work was that the large peculiar velocities measured implied large values of Ω, a result that placed cosmic flows at odds with several other analyses. By the end of the 80's the first attempt to produce a homogeneous catalog by merging different peculiar velocity data set was made (Mark II) and used to obtain the first map of the dark matter in the nearby universe [2]. Even though providing an important first glimpse of the dark matter distribution, this early map showed that important regions of the sky were severely undersampled.

In subsequent years a major effort was made to expand the available sample to confirm the conclusions of the 7S and to improve the mass maps. These efforts included small surveys of specific areas of the sky [7][45] and major TF surveys of spirals, such as those carried out by Matthewson and collaborators [27][28] and the SFI survey [22][23], and FP surveys of early-type galaxies, such as the recently completed ENEAR survey [14]

Trying to capitalize as much as possible on all of the available data, Willick and collaborators[46] assembled the data from these different surveys into a catalog (Mark III) consisting of about 3000 galaxies, predominantly spirals, with measured peculiar velocities. The Mark III catalog, which does not include the more recent all-sky SFI and ENEAR surveys, has been extensively used in the analyses of peculiar velocity data. While considerable effort was made to ensure uniformity, it is a compilation of heterogeneous data sets. As illustrated in figure 11 of Kollat *et al.* [25], it lacks uniformity in sky coverage due to the uneven coverage of the main data sets included in the compilation. While the availability of this catalog prompted the development of several techniques to analyze peculiar velocity data and efforts to understand possible bias, its use has led to conflicting results. The reasons for the discrepancies are not understood and could indicate limitations of the data or of the methods used. Efforts to re-calibrate this catalog using new observations [8] are still underway.

In this context the completion of the SFI I-band TF survey of late spirals and the ENEAR $D_n - \sigma$ survey of early-type galaxies are important additions, providing homogeneous samples of comparable

Figure 1: Projected distribution in Galactic coordinates of ENEAR (top) and SFI(bottom) galaxies.

sizes. Figure 1 shows the projected distribution of galaxies in these two surveys. In contrast to the Mark III compilation, the sky coverage of both surveys is remarkably uniform and nearly all of the data consist of new measurements reduced in a uniform way. Also note that the surveys nicely complement each other: ENEAR galaxies probe high density regions and delineate large-scale structures more sharply; SFI galaxies probe lower density regimes and are more uniformly distributed across the sky. Another important point is that the peculiar velocities in these catalogs are measured using distinct distance estimators based on different observed quantities. Therefore, to take full advantage of these characteristics these samples have been analyzed separately, to test the reproducibility of the results, and combined into the SEcat catalog to produce a fair sample probing a wide range of density regimes. The results of analyses based on these new catalogs of peculiar velocity data are reviewed below and compared to those obtained using Mark III.

4 Results

4.1 Reconstructed density and velocity fields

An underlying assumption of all methods used in estimating β is that galaxies, even though biased, are fair tracers of the mass distribution. This hypothesis can be, in principle, directly tested by comparing the galaxy density field as derived from redshift surveys and the mass density field reconstructed from peculiar velocity data. POTENT, Wiener Filter[49] and more recently the Unbiased Minimal Variance estimator (UMV)[53] are examples of methods developed to reconstruct the three-dimensional velocity and density fields from the observed radial component of the peculiar velocity. All methods assume that on the scales of interest the perturbations are small and non-linear effects can be neglected. The various methods have also been extensively tested using mock catalogs drawn from simulations that mimic the nearby universe.

Recently, the UMV method has been applied to the SEcat catalog of peculiar velocities and to the *PSCz* redshift survey data. Figure 2 shows the map of the PSCz galaxy density field (left panel) and the mass density field (right panel) along the Supergalactic plane, the latter obtained from the SEcat data using a Gaussian smoothing radius of 1200 kms^{-1}. The main features of our local universe are easily identified in these maps, including the Great Attractor (GA) on the left and the Perseus-Pisces supercluster (PP) in the lower right. There is also a hint of the Coma cluster, which lies just outside the volume probed by SEcat, in the upper part on the map. The similarity between the mass and galaxy density fields is striking, especially considering the limitations to the peculiar velocity data imposed by the Zone of Avoidance. Furthermore, even though different in details, the gross features of the mass density field are similar to those obtained by applying either the same or the POTENT formalism to the Mark III catalog[51][17] and SFI catalogs[12]. This is an outstanding result considering the different ways these catalogs were constructed and the peculiar velocities measured. Current results are also a remarkable improvement over those obtained from earlier catalogs. In particular, it is worth mentioning the prominence of the Perseus-Pisces region, completely absent in the earlier maps, and the well-defined voids, well-known features in redshift surveys which are now clearly seen in the reconstructed mass distribution.

The reconstructed three-dimensional velocity field can also be used to measure other quantities of interest. For instance, the amplitude of the bulk flow is found to vary from $V_B = 300\pm$ 70 kms^{-1} for a sphere of $R = 20\,h^{-1}$Mpc to $160\pm$ 60 kms^{-1} for $R = 60\,h^{-1}$Mpc. This value is in good agreement with that obtained from a direct fit to the radial peculiar velocities for the SFI[21] and the ENEAR[15] samples. This result disagrees with the bulk flow determined for the Mark III survey, which has an amplitude of roughly twice this value[51]. The small amplitude of the bulk flow recently measured is in marked contrast to earlier claims of large amplitude coherent motions over scales of the order of $100h^{-1}$ Mpc[7], which at face value would imply excess power on very large scales. This result is in line with the results of recent redshift surveys which have not detected inhomogeneities on very large scales.

Greater insight on the characteristic of the flowfield can be obtained by decomposing the 3-D velocity field into two components, one which is induced by the local mass distribution and a tidal

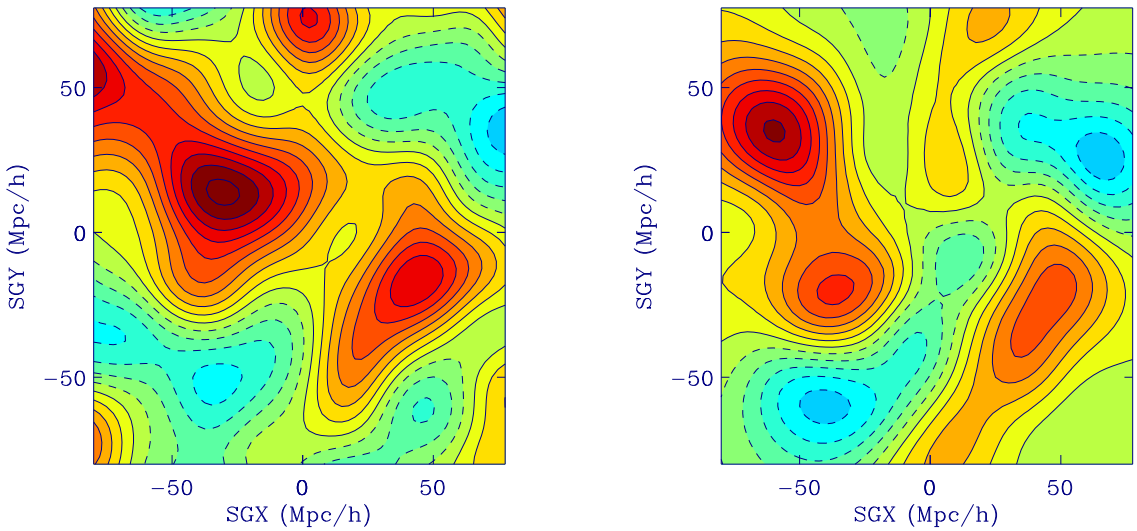

Figure 2: The reconstructed UMV Supergalactic plane density from the *PSCz* (left panel) and the SEcat catalog (right panel) smoothed with $12h^{-1}$ Mpc Gaussian window. The solid and dashed line contours denote positive and negative densities respectively. The bold-solid line denote the zero level density. The contour spacing is 0.1.

Figure 3: Tidal field decomposition of the reconstructed velocity field along the Supergalactic plane displayed as flow lines. The top-left panel shows the full velocity field. The other panels are described in the text.

component due to mass fluctuations external to the volume considered[24][51][52]. Figure 3 shows the results of this decomposition applied to the ENEAR survey[52], where the local volume is a sphere of $80\,h^{-1}$Mpc centered on the Local Group. The plots show the full velocity field (upper left panel), the divergent (upper right panel) and the tidal (lower left panel) components. To further understand the nature of the tidal field, its bulk velocity component has been subtracted and the residual is shown in the lower right panel. This residual is clearly dominated by a quadrupole component. In principle, the analysis of this residual field can shed light on the exterior mass distribution. For the ENEAR catalog we find that the local dynamics is hardly affected by structure on scales larger than its depth. For this sample not only the bulk velocity at large radii is small but so is the *rms* value of the tidal field, estimated to be of the order of 60 kms^{-1}. This is in marked contrast to the results obtained from the analysis of the Mark III survey which yields a much stronger tidal field, pointing (in the sense of its quadrupole moment) towards the Shapley concentration. For Mark III, the tidal field contributes $\sim$ 200 kms^{-1}to the total bulk velocity.

4.2 Estimates of β

Equations (1) and (2) show that there are two alternative ways for estimating β - velocity-velocity or density-density comparisons. In the first case, the observed galaxy distribution is used to infer a mass density field from which peculiar velocities can be predicted and compared to the observed ones. In the second case, the three-dimensional velocity field is obtained from the observed radial velocities and used to infer a self-consistent mass density field and thus a galaxy distribution, via linear biasing. The latter is then compared to the one obtained from large all-sky redshift surveys.

A particularly useful method for performing a velocity-velocity comparison is the modal expansion method[30]. This method expands the velocity fields by means of smooth functions (Bessel and spherical harmonics) defined in redshift space, thus alleviating the Malmquist biases inherent in real space analysis. Furthermore, the modal expansion smooths the observed and predicted velocities in the same way, so that the smoothed fields can be compared directly. Because the number of modes is substantially smaller than the number of data points, the method also provides the means of estimating β from a likelihood analysis carried out on a mode-by-mode basis, instead of galaxy-by-galaxy. The

Figure 4: Comparison of the smoothed velocity fields predicted from the 1.2 Jy *IRAS* survey (left) for an assumed value of $\beta_I = 0.6$ and measured by the SFI redshift-distance survey (right). The velocity fields are shown in redshift shells 2000 kms^{-1} thick.

Figure 5: Comparison of the smoothed velocity fields predicted from the *PSCz IRAS* survey (left), for an assumed value of $\beta_I = 0.5$, and measured by the ENEAR redshift-distance survey (right). The velocity fields are shown in redshift shells 2000 kms^{-1} thick.

similar smoothing and the mode-by-mode comparison substantially simplify the error analysis. The modal expansion method has been used in comparisons between the *IRAS* 1.2 Jy predicted velocities and observed velocities inferred from TF measurements[16] in the Mark III catalog, yielding $\beta_I \sim 0.4$. However, examination of the residual field showed a strong dipole signature suggesting a significant mismatch between the Mark III and the *IRAS* fields. The reasons for the mismatch are still not well-understood.

More recently, the same method has been employed in the comparison of the *IRAS* 1.2 Jy and SFI[9] and of the *IRAS PSCz* and ENEAR velocity fields[31]. Figure 4 shows the smoothed velocity field predicted from the 1.2 Jy *IRAS* survey (left), adopting the best-fit value of $\beta_I = 0.6$, and the measured SFI field (right). The infall to Virgo ($l = 284^\circ, b = 74^\circ$) dominates the nearby SFI flow. In the middle panel, the field exhibits a dipole pattern corresponding to the reflex motion of the Local Group with infalling galaxies in the Hydra-Centaurus direction and an outward flow in the Perseus-Pisces direction, as seen in the LG restframe. Comparing the two fields one immediately sees that the general pattern of the velocity fields is remarkably similar with excellent agreement in the location of outflows and inflows and with only a few nearby galaxies having large residuals. This result gives confidence in the determination of β_I. Most encouraging is the absence of large regions of coherent residuals such as the dipole signature seen in the Mark III analysis at intermediate and distant redshift shells. Similar analysis has been performed using the *PSCz IRAS* survey and the ENEAR catalog of peculiar velocities. Figure 5 shows the corresponding smoothed velocity fields, for an adopted value of $\beta_I = 0.5$. Comparison of the right-side of Figures 4 and 5 shows that the general flow pattern of the SFI and ENEAR velocity fields is remarkably similar. In the ENEAR case, very few prominent structures are probed by bright ellipticals in the innermost shell. However, in the next two shells a strong dipole pattern can be easily recognized, having an amplitude comparable to that observed in SFI. The agreement between the *PSCz* and ENEAR velocity fields is also very good with only a few more distant galaxies having large residuals.

The above results demonstrate that the velocity fields of both SFI and ENEAR are similar and well described by the gravity fields of the *IRAS* 1.2 Jy and *PSCz* surveys, yielding comparable values of β_I. Consistent values of β_I have also been obtained from similar analysis of the SBF survey of galaxy distances ($\beta_I = 0.42$)[3] and from the peculiar velocities measured for a sample of nearby Type Ia supernovae ($\beta_I = 0.4$) [37].

Another method to carry out a velocity-velocity comparison considered is VELMOD, a maximum likelihood method which takes as input the distance indicator observables and galaxy redshifts and determines the parameters describing the distance relation and the velocity model adopted. The method does not require smoothing and it is constructed for high-resolution analysis. The method has been used to analyze sub-samples of spiral galaxies extracted from the Mark III [47][48] and the SFI data[6], yielding $\beta_I = 0.49$ and $\beta_I = 0.42$, respectively. These results show that the value of β_I obtained from velocity-velocity comparisons is independent not only of the data set considered but also of the method used, with all estimates being in the range $0.4 \lesssim \beta_I \lesssim 0.6$.

Unfortunately, until recently there has been a disparity between the results obtained from velocity-velocity comparisons and other methods such as density-density comparisons and maximum-likelihood estimates of the power-spectrum (PS) of mass fluctuations derived from peculiar velocity data [50]. For instance, density-density comparisons using different data sets have invariably led to high values of β[40], consistent with unity. In particular, comparison of the *IRAS* 1.2 Jy and POTENT reconstructed density field, based on the Mark III catalog, yields $\beta_I = 0.89$. Similarly, estimates based on the PS derived from peculiar velocity data using Mark III[50], SFI[19] and ENEAR[52] have yielded values of β in the range 0.82-1.1. The nature of this discrepancy is unknown. Both density-density and velocity-velocity methods have been carefully tested using mock catalogs extracted from N-body simulations and have been shown to provide unbiased estimates of β. Possible reasons for the discrepancy are

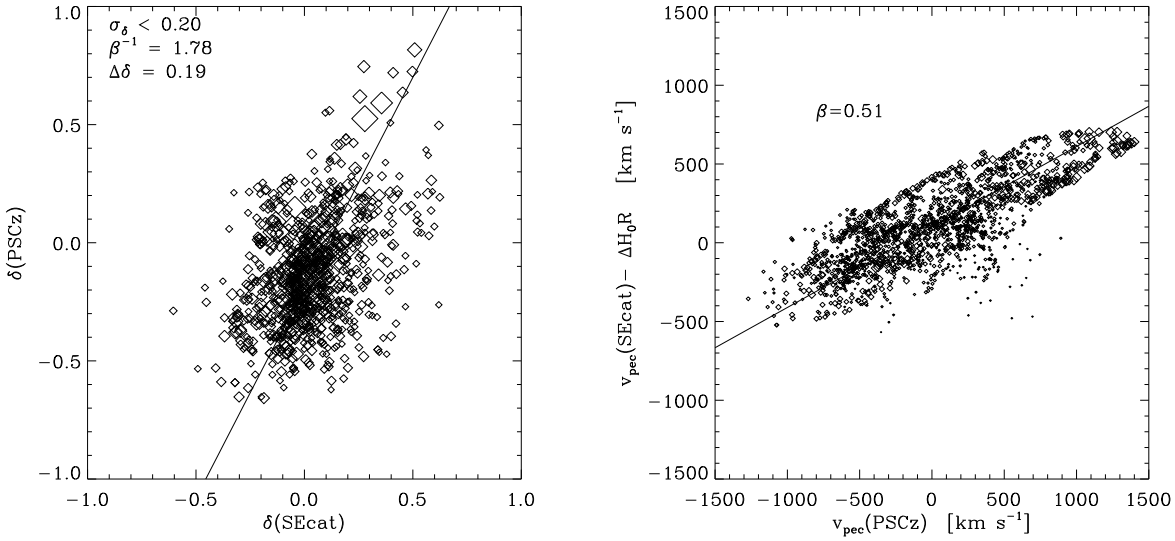

Figure 6: Scatter plots showing the SEcat UMV reconstructed *vs.* the PSCz predicted densities (left panel) and velocities (right panel). The size of the symbols is inversely proportional to the errors

Figure 7: Left panel: Power-spectrum of the most probable COBE-normalized OCDM model estimated for the ENEAR data set compared to those derived from Mark III and SFI samples. Right panel: Contour map of the likelihood for the Γ-model.

non-linear effects, scale dependence of the biasing, poorly understood errors and/or problems with the data. However, attempts to evaluate their impact have so far failed to explain the discrepancy. In general, velocity-velocity comparisons are considered more robust as they depend more on redshift data, while density-density comparisons uses less reliable peculiar velocity data.

Recently, a new attempt to carry out a density-density comparison has been made using the SEcat catalog mentioned earlier and the UMV method to reconstruct the 3-D velocity and density fields. These reconstructed fields were then used to determine the value of β from direct velocity-velocity and density-density comparisons with the corresponding fields predicted from the *PSCz* redshift survey[54]. Figure 6 shows the results of the density-density (left) and velocity-velocity (right) comparisons, which give $\beta_I = 0.56 \pm 0.1$ and $\beta_I = 0.51 \pm 0.05$, respectively. This result is remarkable since it is the first time a good agreement is found for β values derived from these two methods. This encouraging new result, which apparently resolves a long-standing dispute, may be due either to the new method used in the reconstruction of the fields or to the more homogeneous peculiar velocity data used or a combination of both.

High values of β have also been derived from applying a maximum-likelihood technique to the peculiar velocity data to derive the power-spectrum of mass density fluctuations. These results are summarized in Figure 7. In the left panel the PS obtained from the ENEAR sample[52] with those measured for Mark III[50] and SFI[19]. The right panel shows the contour map of the likelihood (in the $\Gamma - \eta_8$ plane) for a Γ model fit to the ENEAR data, where $\eta_8 = \sigma_8 \Omega^{0.6}$ and σ_8 is the rms fluctuation amplitude within a sphere of 8 h^{-1} Mpc radius. It is clear from the figure that all data sets lead to similar high-amplitude PS, equivalent to high values of β. From the figure one also can see that while the likelihood analysis poses a strong constraint on η_8, the value of Γ is poorly determined. Note, however, that low values of Γ, such as those required from the analyses of redshift survey data ($\Gamma \sim 0.2$), are excluded at about the 3σ level.

It is important to recall that the likelihood method used in estimating the PS involves the use of model power-spectra to compute the velocity correlation tensor which is then compared to that computed from the peculiar velocity data to determine the fit parameters. An equivalent way of exploring the same information is to use the scalar velocity correlation function, computed under the assumption of a homogeneous and isotropic flow. The results of this analysis can then be compared directly to model predictions using linear theory and an ensemble average of cosmic flow realizations for different cosmological models. The statistics of the model velocity field is parameterized by the

amplitude, η_8, and by the shape parameter, Γ, of a CDM–like power spectrum. Applying the velocity correlation statistics to the SFI[4] and ENEAR[5] data sets one finds $\eta_8 = 0.34$ (SFI) and $\eta_8 = 0.51$ (ENEAR) for $\Gamma = 0.25$. These values translate to $\beta_I = 0.45 - 0.67$, assuming $b_I/b_o \sim 1.3$, results which agree within the uncertainties with the lower values of β obtained by other methods presented above. More importantly, in contrast to the PS analyses, the region of acceptable solutions comfortably overlaps with other constraints on η_8 derived from the *rms* of cluster peculiar velocities and cluster abundances, and on Γ as determined for the galaxy power spectrum. One possible explanation for the discrepancy between the results of the PS analysis and the velocity correlation statistics is the different way the errors in the distance measurements are taken into account. An important clue is the weak constraint imposed on the shape parameter by the PS analysis. This suggests that the available samples may not be sufficiently deep for this type of analysis, making the method insensitive to the effect that large scale power may have in inducing velocities on small scales.

5 Summary

After considerable effort on both the observational and theoretical fronts, one can state with some degree of confidence that the most controversial issues surrounding large-scale flows are being resolved. The availability of different methods and of data sets have enabled one to test the reproducibility of the results. Especially important has been the completion of modern, homogeneous, all-sky redshift-distance surveys of both spirals and early-type galaxies. These samples probe comparable volumes and allow for independent analyses. Contrary to earlier claims recent analyses yield a small amplitude bulk flow, a mass distribution and velocity field which closely resembles the galaxy density field and the associated gravity field and concordant values of β obtained using different samples, distance indicators and methods. Current constraints argue in favor of a low-density universe and are consistent with those set by galaxy clustering, small-scale dynamics, present-day cluster abundance, high-redshift supernovae and cosmic microwave background. The agreement among such diverse measurements is not only reassuring but gratifying for those who have worked so hard in the field of cosmic flows.

Acknowledgements. I would like to thank all of my collaborators in the SFI and ENEAR projects. Special thanks to S. Zaroubi for many useful discussions.

References

[1] Aaronson, M., Huchra, J., Mould, J., Schechter, P.L. & Tully, R.B., 1982, ApJ, 258, 64

[2] Bertschinger E. & Dekel A. 1989, ApJ, 336, L5

[3] Blakeslee J. *et al.* 2000, in Cosmic Flows 1999: Towards an Understanding of Large-Scale Structures, eds. Courteau S., Strauss M., Willick J. (ASP Conference series) p. 254

[4] Borgani, S., da Costa, L., Zehavi, I., Giovanelli, R., Haynes, M. P., Freudling, W., Wegner, G. & Salzer, J. J., 2000, AJ, 119, 102

[5] Borgani, S., Bernardi, M., da Costa, L., Wegner, G., Alonso, M. V., Willmer, C. N. A., Pellegrini, P. S. & Maia, M. A. G., 2000, ApJ, 537, L1

[6] Branchini E., Freudling, W., da Costa, L., *et al.* , 2001, MNRAS, 326, 1191

[7] Courteau, S., Faber, S., Dressler, A. & Willick, J.A., 1993, ApJ, 412, L51

[8] Courteau, S., Willick, J. A., Strauss, M. A., Schlegel, D. & Postman, M., 2000, ApJ, 544, 636

[9] da Costa, L., Nusser, A., Freudling, W., Giovanelli, R., Haynes, M., Salzer, J. & Wegner, G., 1998, MNRAS, 299, 452

[10] da Costa, L. *et al.* , 1994, ApJ, 424, L1

[11] da Costa, L. N., Vogeley, M. S., Geller, M. J., Huchra, J.P. & Park, C., 1994, ApJ, 437, L1

[12] da Costa, L. N., Freudling, W., Wegner, G., Giovanelli, R., Haynes, M. & Salzer, J., 1996, ApJ, 468, L5

[13] da Costa, L., 1999, in Evolution of Large-Scale Structure from Recombination to Garching, eds. A. J. Banday, R. K. Sheth, L. N. da Costa (Printpartners Ipskamp: Enschede), p.87

[14] da Costa, L. N., Bernardi, M., Alonso, M. V., Wegner, G., Willmer, C. N. A., Pellegrini, P. S., Rité, C. & Maia, M. A. G., 2000, AJ, 120, 95

[15] da Costa, L. N., Bernardi, M., Alonso, M. V., Wegner, G., Willmer, C. N. A., Pellegrini, P. S., Maia, M. A. G. & Zaroubi, S., 2000, ApJ, 537, L81

[16] Davis M., Nusser A. & Willick J. 1996, ApJ 473, 22

[17] Dekel, A., Eldar, A., Kolatt, T., Yahil, A., Willick, J. A., Faber, S. M., Courteau, S. & Burstein, D., 1999, ApJ, 522, 1

[18] Fisher K., Huchra J., Strauss M., Davis M., Yahil A. & Schlegel D. 1995, ApJS, 100, 69

[19] Freudling W, Zehavi, I, da Costa L. N., Dekel A., Eldar A., Giovanelli R., Haynes M. P., Salzer, J. J., Wegner G., Zaroubi S., 1999, ApJ 523, 1.

[20] Geller, M. & Huchra, J., 1989, Science, 246, 857

[21] Giovanelli, R., Haynes, M. P., Freudling, W., da Costa, L. N., Salzer, J. J. & Wegner, G., 1998, ApJ, 505, L91

[22] Haynes, M., Giovanelli R., Salzer J., Wegner, G., Freudling W., da Costa, L., Herter T. & Vogt N., 1999, AJ, 117, 1668

[23] Haynes, M., Giovanelli, R., Chamaraux, P., da Costa, L., Freudling, W., Salzer J. & Wegner, G., 1999, AJ, 117, 2039

[24] Hoffman, Y. Eldar, A., Zaroubi, S., Dekel, A., 2001,, ApJ, *submitted* (astro-ph/0102190).

[25] Kolatt T., Dekel A., Ganon G., Willick J.A., 1996, ApJ, 458, 419

[26] Lynden-Bell, D., Faber, S. M., Burstein, D., Davies, R. L., Dressler, A., Terlevich, R., & Wegner, G. 1988, ApJ, 326, 19

[27] Mathewson D. S., Ford V. L. & Buchhorn M., 1992, ApJS, 81, 412

[28] Mathewson, D. S. & Ford, V. L., 1996, ApJS, 107, 97

[29] Marzke, R. O., Geller, M. J. da Costa, L. N.& Huchra, J. P., 1995, AJ, 110 477

[30] Nusser A. & Davis M. 1994, ApJ, 421, 1L

[31] Nusser, A., da Costa, L. N., Branchini, E., Bernardi, M., Alonso, M. V., Wegner, G., Willmer, C. N. A. & Pellegrini, P. S., 2001, MNRAS, 320, L21

[32] Park, C., Gott, J. R., III & da Costa, L. N., 1992, ApJ, 392, L51

[33] Park, C., Vogeley, M. S., Geller, M. J. & Huchra, J. P., 1994, ApJ, 431, 569

[34] Peacock, J. A. & Dodds, S. J., 1994, MNRAS, 267, 1020

[35] Peacock, J. A., Cole, S., Norberg, P., *et al.* , 2001, Nature, 410, 169

[36] Percival, W. J., Baugh, C. M., Bland-Hawthorn, J. *et al.* , 2001, astro-ph/0105252

[37] Riess A., Davis M., Baker J., Kirschner R. 1997, ApJ 488, L1

[38] Saunders, W., Sutherland, W. J., Maddox, S. J. *et al.* , 2000, MNRAS, 317, 55

[39] Shectman, S. A., *et al.* , 1996, ApJ, 470, 172

[40] Sigad Y., Dekel A., Strauss M. & Yahil A. 1998, ApJ, 495, 516

[41] Strauss, M. A., Huchra, J. P., Davis, M., Yahil, A., Fisher, K. B. & Tonry, J., 1992, ApJS, 83, 29

[42] Strauss M. & Willick J., 1995, Physics Report, 261, 271

[43] Tonry, J.J. & Davis, M., 1981, ApJ, 246, 680

[44] Tonry, J. L., Blakeslee, J. P., Ajhar, E. A. & Dressler, A, 1997, ApJ, 475, 399

[45] Willick, J., 1990, ApJ, 351, L5

[46] Willick J., Courteau S., Faber S., Burstein D., Dekel A. & Strauss M. ApJS, 1997, 109, 333

[47] Willick, J., Strauss, M., Dekel, A. & Kolatt, T. 1997, ApJ, 486, 629

[48] Willick, J. & Strauss, M. 1998, ApJ, 507, 64

[49] Zaroubi, S., Hoffman, Y., Fisher, K. B. & Lahav, O., 1995, ApJ. 449, 446

[50] Zaroubi, S. Zehavi, I., Dekel, A., Hoffman, Y. & Kollat, T., 1997, ApJ, 486, 21

[51] Zaroubi, Hoffman & Dekel, A., 1999, ApJ, 520, 413

[52] Zaroubi, S., Bernardi, M., da Costa, L. N., Hoffman, Y., Alonso, M. V., Wegner, G., Willmer, C. N. A. & Pellegrini, P. S., 2001, MNRAS, 326, 375

[53] Zaroubi, S., 2001, MNRAS, *submitted*

[54] Zaroubi, S., Branchini, E., Hoffman, Y. & da Costa, L., 2001, MNRAS, *submitted*

This figure "dacosta_fig1.gif" is available in "gif" format from:

http://arXiv.org/ps/astro-ph/0110323v1

This figure "dacosta_fig3.gif" is available in "gif" format from:

http://arXiv.org/ps/astro-ph/0110323v1


This figure "dacosta_fig4a.gif" is available in "gif" format from:
http://arXiv.org/ps/astro-ph/0110323v1

This figure "dacosta_fig4b.gif" is available in "gif" format from:

http://arXiv.org/ps/astro-ph/0110323v1

This figure "dacosta_fig5a.gif" is available in "gif" format from:

http://arXiv.org/ps/astro-ph/0110323v1

This figure "dacosta_fig5b.gif" is available in "gif" format from:

http://arXiv.org/ps/astro-ph/0110323v1


This figure "dacosta_fig7a.gif" is available in "gif" format from:
http://arXiv.org/ps/astro-ph/0110323v1

This figure "dacosta_fig7b.gif" is available in "gif" format from:

http://arXiv.org/ps/astro-ph/0110323v1